Biochimica et Biophysica Acta 1798 (2010) 2033–2039

Contents lists available at ScienceDirect

Biochimica et Biophysica Acta

journal homepage: www.elsevier.com/locate/bbamem

Membrane lysis by gramicidin S visualized in red blood cells and giant vesicles

S. Semrau [a,*], M.W.L. Monster [a], M. van der Knaap [b], B.I. Florea [b], T. Schmidt [a], M. Overhand [b]

[a] Physics of Life Processes, Leiden Institute of Physics, Huygens Laboratory, Leiden University, Leiden, The Netherlands
[b] Bio-organic Synthesis, Leiden Institute of Chemistry, Gorlaeus Laboratories, Leiden University, Leiden, The Netherlands

ARTICLE INFO

Article history:
Received 23 January 2010
Received in revised form 15 June 2010
Accepted 5 July 2010
Available online 15 July 2010

Keywords:
Antimicrobial peptide
Gramicidin S
Hemolysis
Giant vesicle
Membrane material parameter

ABSTRACT

The cationic amphiphilic antimicrobial peptide gramicidin S (GS) is an effective antibiotic. Its applicability is however restricted to topical infections due to its hemolytic activity. In this study, the process of GS induced hemolysis was investigated in detail for the first time. The morphological changes of red blood cells (RBCs) inflicted by GS were visualized and explained in terms of a physical model. The observed fast rupture events were further investigated with giant unilamellar vesicles (GUVs) as model systems for RBCs. Measurements of membrane fluctuations in GUVs revealed that the membrane surface tension was increased after incubation with GS. These findings are in agreement with the hypothesis that amphiphilic peptides induce membrane rupture by an increase in membrane tension.

1. Introduction

The amphiphilic decapeptide gramicidin S (GS, Fig. 1) is a cationic antimicrobial peptide that kills Gram-positive bacteria, but is less effective against Gram-negative strains [1]. In combination with an antibiotic targeting Gram-negative bacteria, GS has proven to be an effective antibiotic to treat topical eye and ear infections for more than 50 years [2]. GS does not interact with a specific bacterial gene product but disrupts the bacterial membrane. One key feature in the membrane-disrupting ability of GS is its amphiphilic, detergent-like, secondary structure having amino acid residues with positively charged side-chains positioned on one side of the molecule complemented by residues with hydrophobic side-chains on the opposing side (see Fig. 1) [3–11]. The positively charged side-chains are thought to have electrostatic interactions with the negatively charged lipids of the bacterial membrane, followed by insertion in the bilayer to maximize hydrophobic interactions [3]. The insertion of a cationic antimicrobial peptide such as GS in the bacterial lipid bilayer is accompanied by membrane thinning [4]. Subsequent disruption of the bacterial lipid bilayer was suggested to involve pore formation [5,7,12].

The study presented here is focused on the hemolytic activity of GS, which severely limits the peptide's application range. Understanding the hemolytic process [5] in detail may lead to important clues to the design of less toxic analogs. As shown below, GS caused hemolysis already at low μM concentrations (Section 3.1.1). Red blood cells (RBCs) were found to undergo a distinct sequence of morphological changes (Section 3.1.2) which were interpreted with a physical model (Section 3.1.3). Since the RBCs assumed the shape of spherocytes just prior to rupture, GUVs were used to model the rupture process (Section 3.2.1). Finally, the bending rigidity and membrane tension of GUVs were determined from measurements of membrane fluctuations (Section 3.2.2). The observed increase in membrane tension was consistent with the hypothesis that expanding membrane pores were responsible for membrane rupture.

2. Materials and methods

2.1. Gramicidin S

GS was synthesized following a sequential solid phase synthesis protocol [13] using an Applied Biosystems ABI 433A automated peptide synthesizer on a 200 μmol scale. The Fmoc/Boc protection strategy was followed. The amino acids and coupling reagents were purchased from Novabiochem, and solvents were obtained from Biosolve and used as received from the supplier. LC/MS analyses were performed on a Jasco HPLC-system coupled to Perkin Elmer Sciex API 165 mass instrument with a custom-made electrospray interface. An analytical Alltima C_{18} column (4.6×250 mm, 5 μm) was used in combination with buffers A: H_2O; B: MeCN; and C: 0.5% aqueous trifluoroacetic acid. HPLC purification of GS was conducted with a BIOCAD "Vision" automated HPLC System (Perceptive Biosystems, Inc.) equipped with a preparative Phenomenex C_{18} column (Phenomenex, 21×150 mm, 5 μm). The applied buffers were A: H_2O; B: MeCN; and C: 1% aqueous trifluoroacetic acid, giving GS as its TFA salt in high purity. The spectral data matched those from literature [13].

* Corresponding author.
E-mail address: semrau@physics.leidenuniv.nl (S. Semrau).

0005-2736/$ – see front matter © 2010 Elsevier B.V. All rights reserved.
doi:10.1016/j.bbamem.2010.07.001

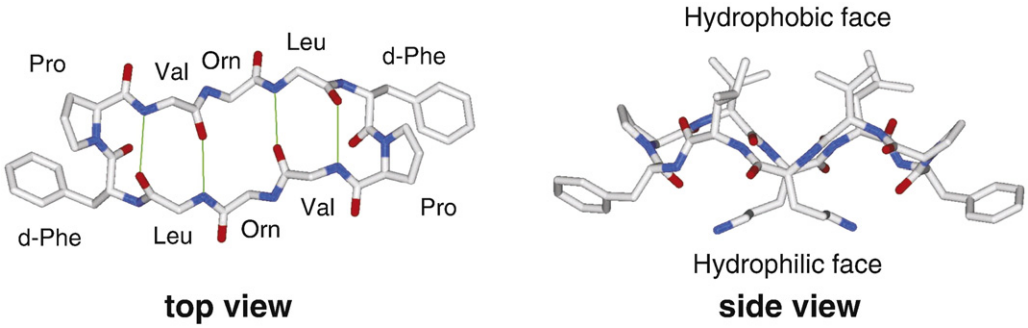

Fig. 1. The X-ray structure of GS ((cyclo-Pro-Val-Orn-Leu-dPhe)2) [10] showing its four intra-molecular hydrogen bonding interactions (top view without side-chains for clarity reasons) and its amphiphilic characteristics, in which the hydrophobic side-chains of the Val and Leu residues are on one side of the molecule and the positively charged side-chains of the two Orn residues on the opposing side (side view).

2.2. RBCs

2.2.1. Preparation

Freshly drawn, heparinized blood was centrifuged for 5 min at 300 rpm. After removing the plasma and the buffy layer containing white blood cells and platelets, the RBCs were washed three times with PBS and stored at 4 °C. The cells were used for about one week.

2.2.2. Dose–response curve

125 µl of RBCs diluted with PBS was transferred to Eppendorf tubes and incubated with 0, 5, 10, 15 and 20 µM of GS, 1% Triton X or 10% v/v ethanol/water, which was the solvent for 20 µM GS. The detergent Triton X is known to cause complete hemolysis and therefore served as a positive control. The RBCs sedimented quickly at the bottom of the tubes. 100 µl of the supernatant was diluted 10× with PBS and the absorption spectrum of the resulting solution between 300 nm and 600 nm was measured with a spectrophotometer (UV-1700 Pharmaspec, Shimadezu, Japan). The absorbance at 415 nm, which corresponds to the absorption maximum of hemoglobin, was taken as a measure for the extent of hemolysis.

2.2.3. Imaging

300 µl of RBCs diluted with PBS was placed in a custom-made sample holder. The PBS was complemented with 0.5% BSA to avoid the "glass effect" [14], which causes RBCs to crenate (i.e., to take the shape of echinocytes) in the proximity of a glass surface. The RBCs were imaged with an inverted wide field microscope (Axiovert 40 CFL, Zeiss, Germany) equipped with a 100× oil-immersion objective ($NA = 1.4$, Zeiss, Germany) and a CCD camera (WAT-902H ULTIMATE, Watec, Orangeburg, USA) connected to a frame grabber (PCI 1405 single channel, National Instruments, USA). The frame grabber was controlled by a homemade LabView program.

2.3. GUVs

2.3.1. Electroformation

GUVs were produced by electroformation using a modified version of the protocol introduced by Angelova et al. [15]. Briefly, lipids dissolved in 9:1 chloroform/methanol were dried under a stream of nitrogen on a glass slide coated with indium tin oxide (ITO). The electroformation chamber consists of this ITO-coated glass, another ITO-coated glass and a polydimethylsiloxane (PDMS) spacer with a thickness of ≈3 mm sandwiched in between. A circular opening of the PDMS spacer around the dried lipids was subsequently filled with the buffer to be contained inside the vesicles. Application of an AC voltage (3.3 V peak to peak, 10 Hz) over night resulted in the formation of GUVs with typical diameters of 10–100 µm. Subsequently, GUVs were harvested, stored at 4 °C and used for several weeks. The buffer enclosed in the vesicles was a 230 mM sucrose solution. For the measurements of the dose response curve and the size distribution (see below) the buffer was supplemented with 6.34 µM Alexa 488 (Invitrogen, Breda, Netherlands). The vesicles were composed of only DOPC lipids (dose–response curve and size distribution experiments) or 99.5% DOPC and 0.5% Rhodamine-DOPE. 1,2-dioleoyl-*sn*-glycero-3-phosphocoline (DOPC) and 1,2-dioleoyl-*sn*-glycero-3-phosphoethanolamine-*N*-(Lissamine Rhodamine B Sulfonyl) (Rhodamine-DOPE) were purchased from Avanti Polar Lipids (Alabaster, USA).

2.3.2. Imaging

10 µl of vesicle-containing solution (harvested from the electroformation chamber) was added to 100–300 µl of a 230 mM glucose solution in a custom-made sample holder. When necessary, GS or $CaCl_2$ were premixed with the glucose solution before addition of the vesicles. The difference in density between the sucrose and glucose solution leads to sedimentation of the vesicles within ≈15 min. The GUVs were imaged with the setup used also for the RBCs (see above). To excite fluorescence of the Rhodamine-DOPE or Alexa 488, samples were illuminated continuously by a mercury lamp (HBO 50, Zeiss) and suitable excitation filters. The fluorescence signal was collected using appropriate dichroic mirrors and emission filters.

2.3.3. Dose–response curve and size distribution

Eppendorf tubes were filled with 100 µl of 230 mM sucrose solution and 20 µl of GUVs containing Alexa 488. Subsequently, various concentrations of GS (0, 1, 2, 3, 5, 7.5,10 µM) and $CaCl_2$ (0, 0.2, 0.4, 0.6, 1, 5, 10 mM) were added. The solutions were left for about 20 min, after which 50 µl of the solution was added to 250 µl of a 230 mM glucose solution in a custom-made sample holder. After sedimentation of the vesicles, about 100 images were taken of each sample. Three hours later the measurement was repeated with 50 µl of the remaining GUV solutions. The big difference of Alexa 488 concentration between the inside and the outside of the vesicles lead to a high image contrast, which made it possible to automatically detect the GUVs. The number and size of the GUVs in every image were automatically determined using MATLAB and a homemade script, which was previously used to identify lipid domains in GUVs [16]. Briefly, fluorescent background is removed by a high pass Fourier filter and the image is converted from grey scale to a binary image by thresholding. Finally, GUVs are identified using standard MATLAB image analysis routines. The average number of GUVs per image and the number of GUVs with a diameter >15 µm was calculated for every concentration and incubation time.

2.3.4. Fluctuation analysis

GUVs composed of 99.5% DOPC and 0.5% Rhodamine-DOPE were transferred to a 230 mM glucose solution. 30 µM Tween 20 was added to the solution to decrease the GUVs' internal pressure. To measure the material parameters of the membranes, short movies of about 3 min at 5 frames per second (and thus approximately 1000 frames) were made of at least ten individual GUVs. These movies were analyzed by a homemade MATLAB routine which traces the vesicles' contours in every frame with a radial accuracy of typically 50–100 nm. From these

contours, the spectra of out-of-plane membrane fluctuations were calculated. Fits of a theoretical description of these fluctuation spectra to the measured data resulted in values for the bending rigidity κ and surface tension σ of the vesicles in the absence or presence of 1 μM GS. Details about the procedure can be found in [17].

3. Results and discussion

3.1. Effect of GS on RBCs

3.1.1. Hemolytic activity

The applicability of GS is restricted to topical infections due to its hemolytic activity. Fig. 2 shows that GS caused hemolysis of RBCs at low μM concentrations. The degree of hemolysis was measured by the amount of hemoglobin released from RBCs.

The observed hemolysis on the time scale of hours therefore could have been either due to a gradual, slow leakage of hemoglobin from all RBCs or from fast disruption of single RBCs. Direct microscopic observation of single RBCs during hemolysis revealed which of these two mechanisms actually took place.

3.1.2. Shape transformation and lysis observed directly

Fig. 3 shows that the RBCs exhibited an intriguing sequence of shape transformations when exposed to 20 μM GS. Starting from the natural discocyte shape, RBC morphology exhibited the sequence echinocyte–discocyte–stomatocyte–discocyte–spherocyte–ghost (Fig. 3A–G), see also Supplementary Movie 1. The very first stage of this sequence has been observed earlier by Katsu and co-workers [5]. The loss of contrast from Fig. 3F to G corresponded to the release of the hemoglobin content of the RBCs, which was completed within tens of seconds. This time scale is consistent with fast, complete rupture of the RBCs, as can be seen from a rough estimation of the diffusion time. If the rupture of the RBC membrane was instantaneous, the time scale for the loss of contrast would be determined by the diffusion coefficient D of hemoglobin. Given $D \approx 10\ \mu m^2/s$ for hemoglobin in RBCs [18] and a cell diameter d of ≈ 10 μm, the time scale t_d for draining of the cell is

$$t_d = \frac{d^2}{6D} \tag{1}$$

so $t_d \approx 2s$, which has the same order of magnitude as the observed time scales. Consequently, a gradual leakage of hemoglobin could be excluded.

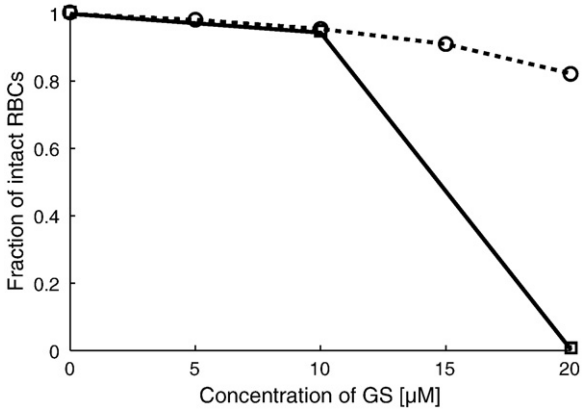

Fig. 2. Hemolytic activity of GS. The graph shows the fraction of intact RBCs after 3 h incubation (open circles and dashed line) and after 24 h incubation (open squares and solid line) with different concentrations of GS dissolved in 10% v/v ethanol/water. At 20 μM of GS all RBCs are lysed after one day. For the pure solvent the fraction of intact RBCs was 0.95 after 3 h and 0.94 after 24 h. These values were determined from the amount of hemoglobin released from RBCs.

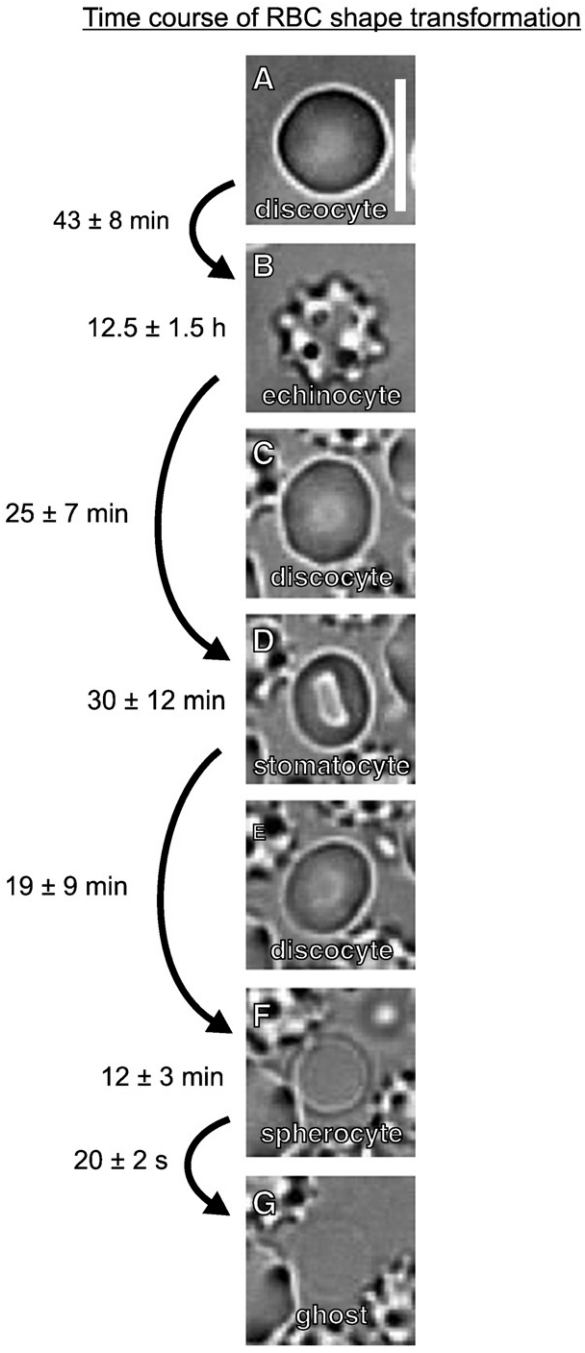

Fig. 3. Shape transformation of RBCs incubated with 20 μM GS. The number of observed cells was N = 12. See also Supplementary Movie 1. Scale bar: 10 μm.

For all experiments on the RBC shape transformations gramicidin S was dissolved in water. When the cells were treated with gramicidin S dissolved in ethanol they exhibited similar shape transformation but it took only minutes for the cells to become crenated and only about 3 h until complete hemolysis (data not shown). This observation seemed to suggest that ethanol had a supportive effect on the hemolytic action of gramicidin S. However, in agreement with earlier studies [19], ethanol turned out to be a crenating agent on its own: minutes after incubation in ethanol only the RBCs transformed to echinocytes (data not shown). Since it was impossible to separate the effect of the solvent from the effect of gramicidin S those experiments were not considered further.

In the following section a model for the shape transformation is presented. This model could explain the observed shape changes by a

minimal physical mechanism without the necessity to invoke specific interactions between GS and cellular proteins.

3.1.3. A tentative model for GS-induced RBC shape transformations

Historically, amphiphilic agents, like GS, were classified into 2 groups based on their effect on RBC shape [20]: compounds which induce the formation of echinocytes and those which give stomatocytes. While the first group contains only anionic or neutral compounds, the second group is comprised of cationic agents. Remarkably, this clear influence of charge on the behavior of amphiphilic compounds could be explained in terms of a physical model, the bilayer coupling model [21,22]. This model relates RBC shape transformations to differences in the area ΔA between the two leaflets of the membrane bilayer. While $\Delta A = 0$ corresponds to the normal, discocyte shape of RBCs, the cells turn into echinocyte when the outer leaflet gets bigger than the inner leaflet ($\Delta A > 0$). In the opposite case ($\Delta A < 0$), RBCs become stomatocytes. The effect of amphiphilic compounds could be understood in terms of the bilayer coupling model because those compounds adsorb to a membrane bilayer at the hydrophilic–hydrophobic interface, thereby expanding the membrane leaflet area (membrane thinning) [23–25]. If the amphiphilic agent adsorbs to the outer membrane leaflet, the bilayer coupling model predicts the formation of echinocytes; if the compounds accumulates in the inner leaflet, RBCs are expected to turn into stomatocytes. A preference for one of the leaflets of the RBC membrane is to be expected due to the difference in charge between the leaflets. The inner leaflet contains more negative lipids [26] (p. 590) and consequently cationic compounds accumulate in this leaflet. Correspondingly, anionic or neutral compounds adsorb preferentially to the outer leaflet. In conclusion, the bilayer coupling model explains the effect of amphiphilic compounds by their membrane area expanding action and their charge-related preferential accumulation in one of the leaflets.

As shown above, GS did not behave according to one of the two groups of amphiphilic compounds, since it caused a sequence of shapes comprising echinocytes and stomatocytes. Still, the bilayer coupling model provided a consistent explanation for the observed shape transformations, which is illustrated in Fig. 4.

First, GS adsorbed to the membrane of an RBC with discocyte shape (Fig. 4A) and expanded the outer leaflet, leading to $\Delta A > 0$ and the transformation of the RBC to an echinocyte (Fig. 4B). The following observed shape (discocyte, see Fig. 4C)) implied that the peptide transiently equilibrated between the two leaflets, resulting in $\Delta A = 0$. The GS might translocate to the inner leaflet by a flip-flop mechanism or the formation of transient pores.

As the inner leaflet of an RBC contains more negatively charged lipids than the outer leaflet [26] (p. 590), GS accumulated in the inner leaflet due to its double positive charge. Because of the resulting higher concentration of GS in the inner leaflet, the area of that leaflet was expanded compared to the inner leaflet, resulting in $\Delta A < 0$ and a stomatocyte shape of the RBC (Fig. 4D). When the inner leaflet was saturated with GS, the outer leaflet filled up with the peptide as well, resulting once again in $\Delta A = 0$ and discocyte RBCs (Fig. 4E). Although not depicted explicitly in Fig. 4 the cytoskeleton of the RBCs played an important role in the observed shape transformations. It was shown earlier that the bilayer-coupling model requires the existence of an elastic membrane skeleton coupled to the membrane for a difference in membrane leaflet area to cause the characteristic shape transformations [22].

The subsequent transformation of the RBCs to spherocytes (Fig. 4E) was beyond the scope of the bilayer coupling model, but could be explained by an increase in membrane tension: it is known that certain amphiphilic peptides [27] increase the membrane tension and thereby the membrane's tendency to minimize its surface area. The observed morphology change of a (flat) discocyte to a spherocyte (Fig. 3E to F) could be related to this effect: a spherical shape minimizes the surface area for a given fixed volume. An increased membrane tension could also explain the final step in the sequence of RBC shape transformations.

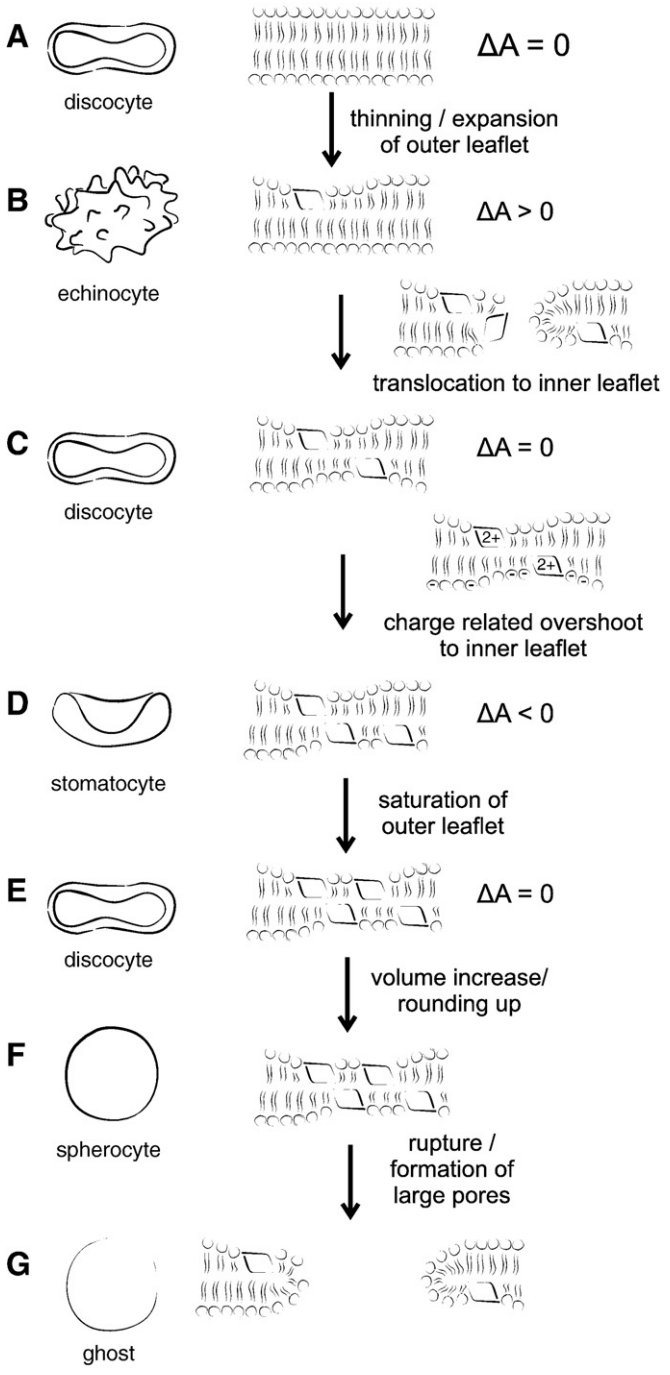

Fig. 4. Tentative model for the shape transformations of RBCs caused by GS.

Membrane pores originating from defects rapidly expanded in the presence of high tension [28], so RBCs ruptured to become ghosts, devoid of hemoglobin (Fig. 4F).

At this point the model presented here, though in agreement with the observed macroscopic phenomena, can only be tentative since independent experimental evidence is required to verify the various stages and elucidate the underlying molecular mechanisms. The following sections of this manuscript zoom in on the very last step, the rupture of spherocytes. Since the complexity of the RBC membrane rendered the identification of the rupture mechanism difficult, GUVs were used as models for spherocytes. GUVs have been used successfully in the past as model systems to study the effect of antibiotic peptides on membranes [29–31].

3.2. Effect of GS on GUVs

3.2.1. Rupture and spreading

GUVs composed of DOPC and filled with the fluorescent dye Alexa 488 were incubated with GS. GUVs were found to rupture only minutes after addition of the compound (see also Supplementary Movie 2a). Fig. 5 shows the rupture of a single GUV in time (see also Supplementary Movie 2b). Leakage of Alexa 488 from GUVs could have resulted from stable pores induced by GS. However, the time scale for complete dispersion of Alexa 488, typically several seconds, was consistent with complete, fast disintegration of the membrane. Alexa 488 has a diffusion coefficient of $D = 430\ \mu m^2/s$ in water [32]. For the vesicle shown in Fig. 5 with a diameter $d \approx 100\ \mu m$ the time scale t_d for draining the vesicle by diffusion is therefore $\approx 4s$, see Eq. (1), which is comparable to the observed time. At none of the used concentrations of GS (0.5 μM–10 μM) was a slower, gradual leakage of Alexa 488 observed. Consequently GS caused – as in the case of the RBCs – fast, complete rupture of the GUV membrane. These observations confirmed earlier studies which showed that GS permeabilizes the membrane without the formation of stable pores [33]. For the experiments presented here it could not be excluded that GS induced stable pores smaller than the size of Alexa 488 (≈ 14 Å [34]). Indeed, in crystals GS forms helical channels of 4.7 Å radius [10]. If such channels formed also in the membrane, Alexa 488 could most probably not pass through. This fact did not diminish the applicability of our model system to the mechanism of GS induced hemolysis. Hemoglobin has a diameter of ≈ 56 Å [18], so any pores too small for Alexa 488 to traverse would presumably also not allow the transport of hemoglobin. Such pores, although irrelevant for the primary rupture mechanism, might still play an important role by facilitating the translocation of GS [27]. In analogy to the pore forming gramicidin A [35] they might also be relevant for the antibiotic action of GS.

In contrast to RBCs GUVs did not exhibit any observable shape transformations prior to rupture. The reason for that lied in the absence of any internal structure of the GUVs. As already mentioned above the bilayer-coupling model requires the existence of an elastic membrane skeleton coupled to the membrane to reproduce all observed RBC shapes [22]. Additionally, GUVs produced by electroformation have initially a high membrane tension [36], evident in the perfectly spherical shape, and no access area available for shape transformations. These characteristics made GUVs suitable models for spherocytes.

The observation of GUVs with a fluorescent membrane provided more evidence for the suggested fast rupture mechanism. Fig. 6(top) shows the time course of a typical rupture event of a GUV exposed to GS. In the depicted GUV, a pore opened (indicated by the arrow in Fig. 6 (top)) on a time scale of 10's of milliseconds and the GUV released a small vesicle trapped inside, see also Supplementary Movie 3. Subsequently, the GUV collapsed and the bilayer spread on the glass surface in a much slower process taking typically 10's of seconds.

While isolated GUVs ruptured and spread on the glass support, groups of vesicles were found to adhere strongly to each other in the presence of GS, see Fig. 6(down). This observation triggered the hypothesis that GS caused vesicle rupture by increasing the adhesion between membrane and glass, and consequently increasing membrane tension. Since GS has a double positive charge, it might have screened repulsive interactions between charged groups on the glass and the dipole moment of the lipids. Ca^{2+} is thought to facilitate the creation of supported bilayers from vesicles by this mechanism [37]. However, a comparison of the dose–response curves for the lysis of GUVs by GS and Ca^{2+}, see Fig. 7, revealed a significant difference between the actions of these molecules. While GS was effective at 1 μM, a 1000-fold higher concentration of Ca^{2+} was needed to cause vesicle rupture. The effect of GS could therefore not be ascribed solely to the charge of the compound and the increased adhesion to the glass support.

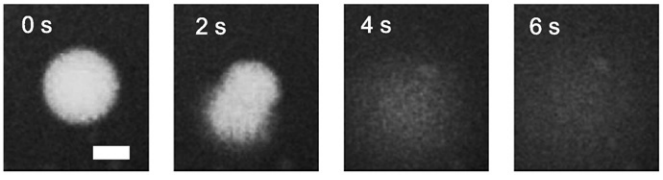

Fig. 5. Time course of rupture of Alexa 488-filled GUV after exposure to 5 μM GS. Scale bar 50 μm. See also Supplementary Movies 2a and b.

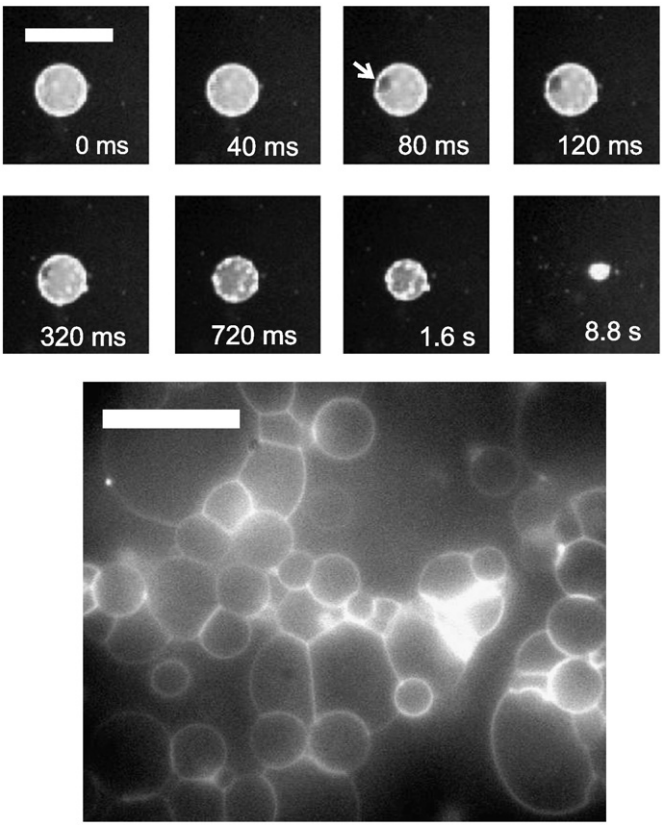

Fig. 6. GUVs labelled with Rhodamine-DOPE incubated with 5 μM GS. Top: Time course of a rupture event. The arrow indicates the opening of a pore. Scale bar 100 μm. Down: Groups of vesicles adhered to each other. Scale bar 25 μm.

In agreement with earlier observations [38], the rupture of GUVs was typically found to be asymmetric, starting from a single point (see Fig. 6 for an example). This observation suggested that GUVs ruptured by formation of a pore which rapidly expanded in the presence of finite membrane tension. As already mentioned above, the insertion of amphiphilic peptides increases the membrane tension, which is accompanied by a thinning of the membrane and an expansion of membrane surface area [27]. This effect has been demonstrated experimentally for helical peptides, like melittin [30], and GS [39]. Measurements of membrane fluctuations described in the following section indicated directly that GS also caused an increase in membrane tension.

3.2.2. Increase in membrane (surface) tension

As shown above, GUVs produced by electroformation already had a high membrane tension and ruptured after exposure to low μM concentrations of GS. To reduce the membrane tension prior to the observation of membrane fluctuations, 30 μM Tween 20 was added to the solution to decrease the GUVs' internal pressure. Tween 20 is a common detergent used to solubilize membrane proteins. At low concentrations, less than the 'critical micellar concentration' (60 μM), it enhances the lifetime of transient membrane pores by reducing the line tension [40]. Incubation with Tween 20 increased the number of GUVs with visible membrane fluctuations, which allowed the measurement of the surface tension σ and the bending rigidity κ from these fluctuations (see also Supplementary Movies 4a and b). In the microscope, the out-

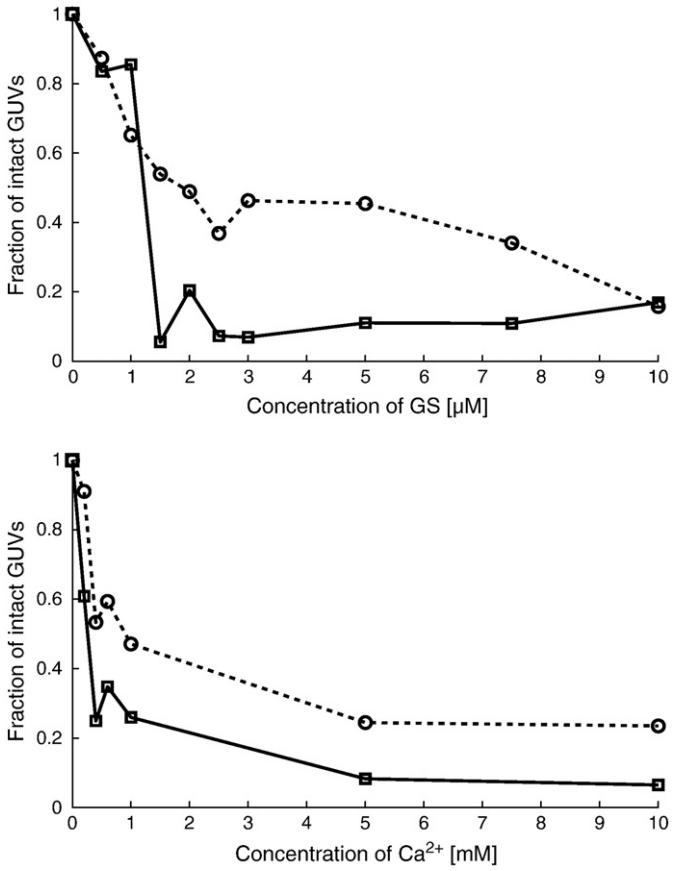

Fig. 7. Up: Dose–response curve for GUVs incubated with GS. Down: Dose–response curve for GUVs incubated with Ca^{2+}. Open symbols, dashed line: immediately after addition of GS; closed symbols, solid line: after 3 h of incubation. Typically 100 images were taken per concentration.

of-plane membrane fluctuations are projected on a plane and can therefore be described by a one-dimensional function $u(s)$, see Fig. 8. $u(s)$ is the deviation of the actual vesicle contour from the average contour with respect to the arc length s. The fluctuation spectra u_q^2 were calculated, where u_q is the Fourier component of $u(s)$ with wave vector q. Fig. 8 compares two typical fluctuation spectra with and without incubation with 1 μM GS.

For an infinite, two-dimensional, flat membrane in thermal equilibrium, the spectrum of out-of-plane fluctuations is

$$\langle |u_q|^2 \rangle = \frac{1}{L^2} \frac{k_B T}{\sigma q^2 + \kappa q^4} \tag{2}$$

where k_B is the Boltzmann constant, $L = 2\pi R$ and R is the vesicle radius. This spectrum follows from the Canham–Helfrich energy [41] and the equipartition theorem, assuming periodic boundary conditions with period L. For small q, so for large wave lengths, the spectrum is dominated by the surface tension σ, while for large q, so short wave lengths, or in the absence of tension, the form of the spectrum only depends on the bending rigidity κ. Due to the finite camera integration time, the measured fluctuations are in fact temporal averages of the real fluctuations, which complicates the spectrum. The complete functional form of the spectrum and its derivation can be found in [17].

A fit of a theoretical model for the expected fluctuation spectra [17] resulted in values for the surface tension σ and bending rigidity κ [17]. The vesicles treated only with Tween 20 ($N = 13$) had on average $\sigma = 2.4 \pm 0.8 \cdot 10^{-7}\,\mathrm{J/m^2}$ and $\kappa = 1.8 \pm 0.7 \cdot 10^{-19}\,\mathrm{J}$. The vesicles treated additionally with 1 μM GS ($N = 21$) had on average $\sigma = 6.3 \pm 1.7 \cdot 10^{-7}\,\mathrm{J/m^2}$ and $\kappa = 1.8 \pm 0.7 \cdot 10^{-19}\,\mathrm{J}$. Surprisingly, the bending rigidity

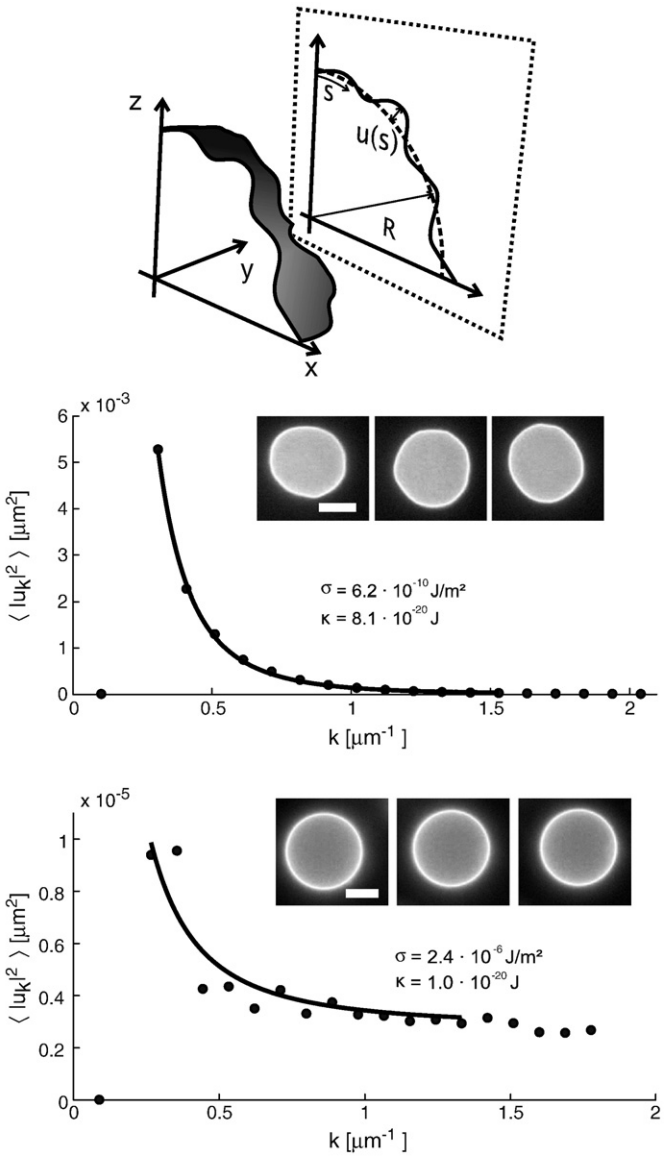

Fig. 8. Determination of membrane material parameters from membrane fluctuations. The out-of-plane membrane fluctuations projected by the microscope on a plane $u(s)$ with respect to the arc length s. Typical GUV fluctuation spectra without (center) and with (down) addition of 1 μM GS. The insets show snapshots taken from the corresponding vesicles, the scale bar is 10 μm. See also Supplementary Movies 4a and b. A fit of the theoretical model of membrane fluctuations resulted in $\sigma = 6.2 \cdot 10^{-10}\,\mathrm{J/m^2}$, $\kappa = 8.1 \cdot 10^{-20}\,\mathrm{J}$ (center) and $\sigma = 2.4 \cdot 10^{-6}\,\mathrm{J/m^2}$, $\kappa = 8.1 \cdot 1.0^{-20}\,\mathrm{J}$ (down).

remained constant within experimental accuracy. Theoretical calculations predict an increase in bending rigidity if amphiphilic peptides are adsorbed to the bilayer [42]. The membrane tension, on the other hand, was significantly increased due to GS exposure. Such an increase in tension might promote the expansion of a pore, which would lead to rupture.

4. Conclusion

In conclusion we have presented the shape transformation of RBCs upon exposure to GS and suggested a purely physical interpretation based on the bilayer coupling model. Similar morphology changes were observed with the helical amphiphilic peptide melittin [43]. Despite the structural difference of GS and melittin, their effect on the RBC shape was comparable (see also [5]), which suggests that the observed hemolytic process is generic for amphiphilic peptides and independent of the structure of a particular peptide. We have furthermore zoomed in

on the last stage of hemolysis, the rupture of spherocytes, which were modelled by GUVs. Most importantly, the membrane tension was determined from thermal membrane fluctuations and found to increase upon incubation with GS. These observations were in agreement with earlier studies with other amphiphilic peptides [27,30,31]. In the literature, there is a controversy whether GS disrupts membranes by pore formation [5,7,12]. Of importance is not only whether pores are formed, but in which stages of the membrane disruption process. The observations described here lead to the hypothesis that GS did not form stable pores due to the presence of a finite membrane tension. This tension overcompensated the tendency of the pore to close [27,28], which lead to expansion of the pore and complete rupture. Why GS is different in this respect from other peptides, which indeed form stable pores, is at present still unclear. The exact nature of the mechanism and the dynamics of pore formation of GS and related peptides will be unravelled with the help of single-molecule fluorescence experiments in mammalian and bacterial cells.

Acknowledgements

This work is part of the research program of the Stichting voor Fundamenteel Onderzoek der Materie (FOM), which is financially supported by the Nederlandse organisatie voor Wetenschappelijk Onderzoek (NWO) within the program on Material Properties of Biological Assemblies (Grant FOM-L1707M).

Appendix A. Supplementary data

Supplementary data associated with this article can be found, in the online version, at doi:10.1016/j.bbamem.2010.07.001.

References

[1] G.F. Gause, M.G. Brazhnikova, Gramicidin S and its use in the treatment of infected wounds, Nature 154 (0) (1944) 703.
[2] C.J. Wadsten, C.A. Bertilson, H. Sieradzki, and S. Edstrom. A randomized clinical trial of two topical preparations (framycitin/gramicidin and oxytetracycline/hydrocortisone with polymyxin b) in the treatment of external otitis. *Archives of Oto-Rhino-Laryngology-Archiv Für Ohren-Nasen-Und Kehlkopfheilkunde*, 242:0 135, 1985.
[3] A.S. Kaprelyants, V.V. Nikiforov, A.I. Miroshnikov, L.G. Snezhkova, V.A. Eremin, D. N. Ostrovskii, Membranes of bacteria and mechanism of action of the antibiotic gramicidin S, Biochem. (Moscow) 42 (0) (1977) 329–337.
[4] S.E. Hull, R. Karlsson, P. Main, M.M. Woolfson, E.J. Dodson, The crystal structure of a hydrated gramicidin S-urea complex, Nature 275 (0) (1978) 206–207.
[5] T. Katsu, M. Kuroko, T. Morikawa, K. Sanchika, Y. Fujita, H. Yamamura, M. Uda, Mechanism of membrane damage induced by the amphipathic peptides gramicidin S and melittin, Biochim. Biophys. Acta 983 (0) (1989) 135–141.
[6] E.J. Prenner, R.N.A.H. Lewis, R.N. McElhaney, The interaction of the antimicrobial peptide gramicidin S with lipid bilayer model and biological membranes, Biochim. Biophys. Acta 1462 (0) (1999) 201–221.
[7] M. Wu, E. Maier, R. Benz, R.E.W. Hancock, Mechanism of interaction of different classes of cationic antimicrobial peptides with planar bilayers and with the cytoplasmic membrane of *Escherichia coli*, Biochemistry 38 (0) (1999) 7235.
[8] J. Salgado, S.L. Grage, L.H. Kondejewski, R.S. Hodges, R.N. McElhaney, A.S. Ulrich, Membrane-bound structure and alignment of the antimicrobial b-sheet peptide gramicidin S derived from angular and distance constraints by solid-state 19f-NMR, J. Biomol. NMR 21 (0) (2001) 191–208.
[9] G.M. Grotenbreg, M.D. Witte, P.A.V. van Hooft, E. Spalburg, P. Reiss, D. Noort, A.J. de Neeling, U. Koert, G.A. van der Marel, H.S. Overkleeft, M. Overhand, Synthesis and biological evaluation of gramicidin S dimers, Org. Biomol. Chem. 3 (0) (2005) 233–238.
[10] A.L. Llamas-Saiz, G.M. Grotenbreg, M. Overhand, M.J. van Raaij, Double-stranded helical twisted beta-sheet channels in crystals of gramicidin S grown in the presence of trifluoroacetic and hydrochloric acids, Acta Cryst. D 63 (0) (2007) 401–407.
[11] S. Afonin, U.H.N. Dürr, P. Wadhwani, J. Salgado, A.S. Ulrich, Solid state NMR structure analysis of the antimicrobial peptide gramicidin S in lipid membranes: concentration-dependent re-alignment and self-assembly as a §-barrel, Top. Curr. Chem. 273 (0) (2008) 139–154.
[12] G.M. Grotenbreg, M.S.M. Timmer, A.L. Llamas-Saiz, M. Verdoes, G.A. van der Marel, M. J. van Raaij, H.S. Overkleeft, M. Overhand, An unusual reverse turn structure adopted by a furanoid sugar amino acid incorporated in gramicidin s, J. Am. Chem. Soc. 126 (0) (2004) 3444.
[13] G.M. Grotenbreg, M. Kronemeijer, M.S.M. Timmer, F. El Oualid, R.M. van Well, M. Verdoes, E. Spalburg, P.A.V. van Hooft, A.J. de Neeling, D. Noort, J.H. van Boom, G.A. van der Marel, H.S. Overkleeft, M. Overhand, A practical synthesis of gramicidin S and sugar amino acid containing analogues, J. Org. Chem. 69 (0) (2004) 7851–7859.
[14] L.E. Göran Eriksson, On the shape of human red blood cells interacting with flat artificial surfaces — the 'glass effect', Biochim. Biophys. Acta 1036 (0) (1990) 193–201.
[15] M.I. Angelova, D.S. Dimitrov, Liposome electroformation, Faraday Discuss. Chem. S. 81 (0) (1986) 303–311.
[16] S. Semrau, T. Idema, T. Schmidt, C. Storm, Membrane-mediated interactions measured using membrane domains, Biophys. J. 96 (0) (2009) 4906–4915.
[17] S. Semrau, T. Idema, L. Holtzer, T. Schmidt, C. Storm, Accurate determination of elastic parameters for multicomponent membranes, Phys. Rev. Lett. 1000 (8) (2008) 088101.
[18] W. Doster, L. Stéphane, Microscopic diffusion and hydrodynamic interactions of hemoglobin in red blood cells, Biophys. J. 93 (0) (2007) 1360–1368.
[19] R.W. McLawhon, Y. Marikovsky, R.S. Weinstein, Ethanol-induced alterations in human erythrocyte shape and surface properties: modulatory role of prostaglandin E_1, J. Mem. Biol. 99 (0) (1987) 73–78.
[20] B. Deuticke, Transformation and restoration of biconcave shape of human erythrocytes induced by amphiphilic agents and changes of ionic environment, Biochim. Biophys. Acta 163 (0) (1968) 494–500.
[21] M.P. Sheetz, S.J. Singer, Biological membranes as bilayer couples. A molecular mechanism of drug-erythrocyte interactions, Proc. Natl Acad. Sci. USA 71 (0) (1974) 4457–4461.
[22] G.H.W. Lim, M. Wortis, R. Mukhopadhyay, Stomatocyte–discocyte–echinocyte sequence of the human red blood cell: evidence for the bilayer-couple hypothesis from membrane mechanics, Proc. Natl Acad. Sci. USA 99 (0) (2002) 16766–16769.
[23] Y. Wu, K. He, S.J. Ludtke, H.W. Huang, X-ray diffraction study of lipid bilayer membranes interacting with amphiphilic helical peptides: diphytanoyl phosphatidylcholine with alamethicin at low concentrations, Biophys. J. 68 (0) (1995) 2361–2369.
[24] S. Ludtke, K. He, H.W. Huang, Membrane thinning caused by magainin 2, Biochemistry 34 (0) (1995) 16764–16769.
[25] A. Mecke, D.-K. Lee, A. Ramamoorthy, B.G. Orr, M.M.B. Holl, Membrane thinning due to antimicrobial peptide binding: an atomic force microscopy study of msi-78 in lipid bilayers, Biophys. J. 89 (0) (2005) 4043–4050.
[26] B. Alberts, D. Bray, J. Lewis, M. Raff, K. Roberts, J.D. Watson, Molecular Biology of the Cell, 4 edition, Garland Publishing, 1994.
[27] H.W. Huang, Molecular mechanism of peptide-induced pores in membranes, Phys. Rev. Lett. 92 (0) (2004) 198304.
[28] E. Karatekin, O. Sandre, F. Brochard-Wyart, Transient pores in vesicles, Polym. Int. 52 (0) (2003) 486–493.
[29] E.E. Ambroggio, F. Separovic, J.H. Bowie, G.D. Fidelio, L.A. Bagatolli, Direct visualization of membrane leakage induced by the antibiotic peptides: maculatin, citropin and aurein, Biophys. J. 89 (0) (2005) 1874–1881.
[30] M.L. Longo, A.J. Waring, L.M. Gordon, D.A. Hammer, Area expansion and permeation of phospholipid membrane bilayers by influenza fusion peptides and melittin, Langmuir 14 (0) (1998) 2385–2395.
[31] M.-T. Lee, W.-C. Hung, F.-Y. Chen, H.W. Huang, Mechanism and kinetics of pore formation in membranes by water-soluble amphipathic peptides, Proc. Natl Acad. Sci. USA 105 (0) (2008) 5087–5092.
[32] J.M. Nitsche, H.-C. Chang, P.A. Weber, B.J. Nicholson, A transient diffusion model yields unitary gap junctional permeabilities from images of cell-to-cell fluorescent dye transfer between xenopus oocytes, Biophys. J. 86 (0) (2004) 2058–2077.
[33] Md. Ashrafuzzaman, O.S. Andersen, R.N. McElhaney, The antimicrobial peptide gramicidin S permeabilizes phospholipid bilayer membranes without forming discrete ion channels, Biochim. Biophys. Acta 1778 (0) (2008) 2814–2822.
[34] A. Masuda, K. Ushida, T. Okamoto, New fluorescence correlation spectroscopy enabling direct observation of spatiotemporal dependence of diffusion constants as an evidence of anomalous transport in extracellular matrices, Biophys. J. 88 (0) (2005) 3584–3591.
[35] S.B. Hladky, D.A. Haydon, Ion transfer across lipid membranes in the presence of gramicidin A, BBA 274 (0) (1972) 294–312.
[36] R. Dimova, S. Aranda, N. Bezlyepkina, V. Nikolov, K.A. Riske, R. Lipowsky, A practical guide to giant vesicles. probing the membrane nanoregime via optical microscopy, J. Phys. Condens. Matter 28 (0) (2006) S1151–S1176.
[37] Y.-H. Kim, Md.M. Rahman, Z.-L.-. Zhang, N. Misawa, R. Tero, T. Urisu, Supported lipid bilayer formation by the giant vesicle fusion induced by vesicle–surface electrostatic attractive interaction, Chem. Phys. Lett. 420 (0) (2006) 569–573.
[38] C. Hamai, P.S. Cremer, S.M. Musser, Single giant vesicle rupture events reveal multiple mechanisms of glass-supported bilayer formation, Biophys. J. 92 (0) (2007) 1988–1999.
[39] E. Staudegger, E.J. Prenner, M. Kriechbaum, G. Degovics, R.N.A.H. Lewis, R.N. McElhaney, K. Lohner, X-ray studies on the interaction of the antimicrobial peptide gramicidin S with microbial lipid extracts: evidence for cubic phase formation, BBA-Biomembr. 14680 (1–2) (2000) 213–230.
[40] N. Borghi, S. Kremer, V. Askovic, F. Brochard-Wyart, Tube extrusion from permeabilized giant vesicles, Europhys. Lett. 75 (0) (2006) 666–672.
[41] W. Helfrich, Elastic properties of lipid bilayers: theory and possible experiments, Z. Naturforsch. C 28 (0) (1973) 693–703.
[42] A. Zemel, A. Ben-Shaul, S. May, Modulation of the spontaneous curvature and bending rigidity of lipid membranes by interfacially adsorbed amphipathic peptides, J. Phys. Chem. B 112 (0) (2008) 6988–6996.
[43] M.T. Tosteson, S.J. Holmes, M. Razin, D.C. Tosteson, Melittin lysis of red cells, J. Memb. Biol. 87 (0) (1985) 35–44.